Modeling and Numerical Simulation of a Two-Dimensional MPD thruster using a Hydrogen Propellant

IEPC-2011-258

Presented at the 32nd International Electric Propulsion Conference,
Wiesbaden • Germany
September 11 – 15, 2011

H. Sato[1]
The Graduate University for Advanced Studies, Sagamihara, Kanagawa, 252-5210, Japan

K. Kubota[2]
Japan Aerospace Exploration Agency, Chofu, Tokyo, 182-8522, Japan

and

I. Funaki[3]
Japan Aerospace Exploration Agency, Sagamihara, Kanagawa, 252-5210, Japan

Abstract: Numerical model considering the ion-slip effect is built and numerical simulation is conducted for the two-dimensional magnetoplasmadynamic thruster (2D-MPDT, flared type, H_2 propellant). The calculation condition is set to the mass flow rate of 0.65 g/s and the total discharge current of 13 kA. Compared to the numerical simulation without the ion-slip effect, the numerical simulation with the ion-slip effect can reproduce the measured result (discharge current path, electron temperature, translational temperature, thrust performance) relatively well. The numerical thrust performance shows F = 22.1 N, P_e = 951 kW (measured F = 27.0 N, P_e = 1,521 kW). The ion-slip effect causes near the anode (ion-slip parameter S_{ion} > 1), because the plasma flow is kept low ionization degree and low pressure due to the pinched force. The translational temperature exceeds the electron temperature around the corner of the anode within the discharge chamber due to the heating of the ion-slip effect.

Nomenclature

B	=	magnetic flux vector
E	=	energy
e	=	elementary electric charge
I	=	unit matrix
j	=	current density vector
J_{dis}	=	total discharge current
m_{aton}	=	mass of hydrogen atom
$\dot{m}$	=	mass flow rate
n	=	number density
$Qi\text{-}j$	=	relaxation term between energy mode i and j
T	=	temperature

[1] Graduate Student, Department of Space and Astronautical Science, satoh.hiroki@jaxa.jp.
[2] Researcher, Aerospace Research and Development Directorate, kubota.kenichi@jaxa.jp.
[3] Associate Professor, Institute of Space and Astronautical Science, funaki@isas.jaxa.jp.

p	=	pressure
R	=	gas constant
S_{ion}	=	ion-slip parameter
t	=	time
u	=	velocity vector
V_{diss}	=	dissociation energy (= 4.4 eV)
V_{ion}	=	ionization energy(= 13.6 eV)
x, y	=	cartesian coordinate (for physical space)
α	=	ionization fraction
β	=	Hall parameter
ρ	=	mass density
θ_{vib}	=	characteristic temperature for vibration (= 6,320 K)
ξ, η	=	Generalized coordinate (for computational space)
ξ_s, η_s	=	partial differential $\partial\xi/\partial s$, $\partial\eta/\partial s$

Subscript

e	=	electron
h	=	heavy particle
i	=	ion
ref	=	reference value
rot	=	rotational mode
tr	=	translational mode
vib	=	vibrational mode

I. Introduction

A self-field magnetoplasmadynamic thruster (MPDT)[1] is a form of electric propulsion for spacecrafts, which its thrust is produced by Lorentz force. The arc discharge current J (~ 1 – 20 kA) ionizes a gaseous propellant and produces a Lorentz force (**J**×**B**) in the discharge chamber of MPDT. The MPDT can produce a high thrust density (~10^4 N/m^2) and a high specific impulse (> 2,000 sec) at high power operation. Although the MPDT is expected to used as a main thruster of large spacecraft, it faces a problem of low thrust efficiency (20-30%)[2,3] in the case of noble gas (e.g., argon, xenon) propellant. Utilization of hydrogen as a propellant is a solution to improve thrust efficiency of the MPDT. Uematsu[2] found that his hydrogen MPD is superior to that using other propellants. The ion-slip (velocity slip between neutral particles and ions), however, is experimentally observed within the MPDT using the molecular propellant. Malliaris[4] observed the ion-slip within the coaxial MPDT using the ammonia propellant. Recently, Kinefuchi[5] also observed the ion-slip within the two-dimensional MPDT (Fig. 1) using the hydrogen propellant, but its cause and the influence on the thrust performance hasn't been cleared yet. The ion-slip should be investigated by the numerical simulation, because only experimental study can't measure plasma quantity within the entire discharge chamber. Although the MPDT using the argon propellant was simulated numerically (one-dimension) [7,8] with the ion-slip, the MPDT using the hydrogen propellant hasn't been simulated numerically with the ion-slip yet.

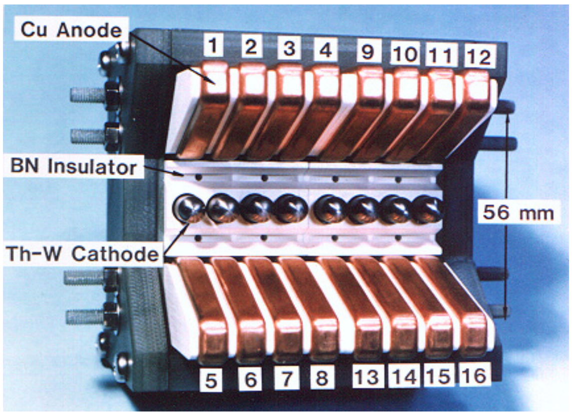

Figure 1. Two-dimensional MPDT (exhaust plane).

In order to reveal the cause of the ion-slip effect and the its influence on the plasma flow within the MPDT using the hydrogen propellant, the numerical model considering the ion-slip effect is built and the two-dimensional numerical simulation using its model is conducted for the two-dimensional MPDT (Fig. 1, flared type). First, the numerical result with the ion-slip effect is compared with the numerical result without the ion-slip and the measured result to validate the numerical model considering the ion-slip effect. Finally, the cause of the ion-slip effect and its influence on the plasma flow is revealed.

II. Modeling

A. Assumptions

The following assumptions are employed in this numerical simulation.

- The plasma flow is treated as the magnetohydrodynamic flow with real gas effects.
- Hydrogen was used as the propellant.
- Hydrogen molecular H_2, atom H, ion H^+, and electron are considered as species.
- The flow field is uniform in z-direction (depth-direction in Fig. 2, $\partial/\partial z = 0$).
- Only a z-direction component B_z (self-field) was considered in the magnetic field.
- Turbulent was ignored.
- Sheath drop voltage was ignored.
- Viscous, heat conduction, nonequilibrium dissociation and ionization were incorporated.
- A translational for heavy particles, a vibrational for H_2 and a translational for the electron temperature were treated separately.

(with ion-slip effect)

- The Hall effect and the ion-slip effect are considered in the generalized Ohm's law which is written as Eq. (A.1) in Appendix A. The gradient of electron pressure is ignored in the generalized Ohm's law.

(w/o ion-slip effect)

- The Hall effect is considered in the generalized Ohm's law. The ion-slip effect and the gradient of electron pressure are ignored in the generalized Ohm's law.

B. Basic equations

The governing equations for the plasma flow in the MPDT using the hydrogen propellant are the mass conservation of the total, hydrogen atom, and ion, the momentum conservation, and the energy conservation of the heavy particle, the vibration, and the electron (referred from Appendix B). The equations are as follows.

$$\frac{\partial \rho}{\partial t} + \nabla \cdot (\rho \mathbf{u}) = 0 \tag{1}$$

$$\frac{\partial \rho_s}{\partial t} + \nabla \cdot (\rho_s \mathbf{u}) = \dot{\rho}_s \quad (s = \mathrm{H}, \mathrm{H}^+) \tag{2}$$

$$\frac{\partial \rho \mathbf{u}}{\partial t} + \nabla \cdot (\rho \mathbf{u}\mathbf{u} + p\mathbf{I}) = \mathbf{j} \times \mathbf{B} + \nabla \cdot \boldsymbol{\tau} \tag{3}$$

$$\begin{aligned} &\frac{\partial E_h}{\partial t} + \nabla \cdot \left[(E_h + p)\mathbf{u} \right] \\ &= p_e \nabla \cdot \mathbf{u} + \mathbf{u} \cdot (\mathbf{j} \times \mathbf{B}) + \frac{S_{ion}}{\sigma |\mathbf{B}|^2} (\mathbf{j} \times \mathbf{B})^2 + \nabla \cdot ((\lambda_{tr} + \lambda_{rot}) \nabla T_{tr}) + \nabla \cdot (\lambda_{vib} \nabla T_{vib}) + \nabla \cdot (\boldsymbol{\tau} \mathbf{u}) - Q_{tr-e} + Q_{e-vib} - Q_{diss}^h \end{aligned} \tag{4}$$

$$\frac{\partial E_{vib}}{\partial t} + \nabla \cdot \left[E_{vib} \mathbf{u} \right] = \nabla \cdot (\lambda_{vib} \nabla T_{vib}) + Q_{tr-vib} + Q_{e-vib} - Q_{diss}^h \tag{5}$$

$$\frac{\partial E_e}{\partial t} + \nabla \cdot \left[E_e \mathbf{u} \right] = -p_e \nabla \cdot \mathbf{u} + \frac{\mathbf{j}^2}{\sigma} + \nabla \cdot (\lambda_e \nabla T_e) + Q_{tr-e} - Q_{e-vib} - Q_{diss}^e - Q_{ion}^e \tag{6}$$

The production rate equations of hydrogen atom and ion in the right-hand side of Eq. (2) are given by

$$\dot{\rho}_H = \sum_{s=1}^{4} 2\left(k_{f,s} n_{H_2} - k_{b,s} n_H^{\ 2}\right) n_s m_{atom} - \left(k_{f,s} n_H n_e - k_{b,s} n_{H^+} n_e^2\right) m_{atom} \tag{7}$$

$$\dot{\rho}_{H^+} = \left(k_{f,5} n_H n_e - k_{b,5} n_{H^+} n_e^2\right) m_{atom} \tag{8}$$

where the forward reaction coefficient k_f and the recombination coefficient k_b were referred from Fujita[9] and Shoji[10], respectively. The viscous tensor $\boldsymbol{\tau}$ is given by

$$\boldsymbol{\tau} = \mu\left(\frac{\partial u_i}{\partial x_j} + \frac{\partial u_j}{\partial x_i} - \frac{2}{3}\delta_{ij}\frac{\partial u_k}{\partial x_k}\right) \tag{9}$$

The energy of the heavy particle and the electron are defined as

$$E_h = E_{tr} + E_{rot} + E_{vib} + \frac{1}{2}\rho\mathbf{u}^2 = \frac{3}{2}\sum_{s\neq e}\rho_s R_s T_{tr} + \rho_{H_2} R_{H_2} T_{tr} + \frac{\rho_{H_2} R_{H_2}\theta_{vib}}{\exp(\theta_{vib}/T_{vib}) - 1} + \frac{1}{2}\rho\mathbf{u}^2 \tag{10}$$

$$E_e = \frac{3}{2} n_e k T_e = \frac{3}{2} p_e \tag{11}$$

The third term of the right hand side in Eq. (4) represents the ion-slip effect. An ion-slip parameter S_{ion} is obtained from the following equation[11].

$$S_{ion} = \begin{cases} (1-\alpha)^2 \beta_e \beta_{in} & \text{(with ion - slip effect)} \\ 0 & \text{(w/o ion - slip effect)} \end{cases} \tag{12}$$

When the ion-slip effect is ignored, the ion-slip parameter is assumed $S_{ion} = 0$. The electric Hall parameter β_e and the ion Hall parameter β_{in} is obtained from

$$\beta_e = \frac{e|B_z|}{m_e \nu_{es}} = \frac{\sigma |B_z|}{e n_e} \tag{13}$$

$$\beta_{in} = \frac{e|B_z|}{m_i \nu_{in}} = \frac{e|B_z|}{m_i \left(n_{H_2} + n_H\right) Q_{in}\sqrt{8kT_{tr}/\pi m_i}} \tag{14}$$

The governing equation for the self-field in the MPDT is the induction equation.

$$\frac{\partial \mathbf{B}}{\partial t} - \nabla \times (\mathbf{u}\times\mathbf{B}) = -\nabla \times \left\{\frac{1}{\mu_0 \sigma}\nabla\times\mathbf{B} + \frac{1}{\mu_0 e n_e}(\nabla\times\mathbf{B})\times\mathbf{B}\right\} + \nabla\times\left\{\frac{S_{ion}}{\mu_0\sigma|\mathbf{B}|^2}\left((\nabla\times\mathbf{B})\times\mathbf{B}\right)\times\mathbf{B}\right\} \tag{15}$$

The respective first, second, and third term of the right hand side in Eq. (15) represents the magnetic diffusion, the Hall effect, and the ion-slip parameter.

The remaining relational expression necessary for the complete formulation are the equation of state and the Ampère's law:

$$p = \sum_{s\neq e} n_s k T_{tr} + n_e k T_e \tag{16}$$

$$\mathbf{j} = \frac{1}{\mu_0}\nabla\times\mathbf{B} \tag{17}$$

The evaluation methods of the viscosity coefficient μ, the thermal conductivity λ_s and the electric conductivity σ are referred from Gnoffo[12]. Then, the integral collision is referred from Yos[13] and Stallcop[14].

III. Numerical Procedure

A. Calculation method

The governing equations are discretized spatially by the finite volume method. The convective flux is evaluated by 2nd-order TVD Lax-Friedrich scheme with the minmod limited function[15]. In addition, the dissipative flux is evaluated by a central-difference scheme. The convergence solution is obtained by the time-marching method with 1st-order Euler explicit method. Only time integral of the magnetic diffusion term is computed by the diagonal point implicit method.

B. Computational domain and thruster geometry

Figure 2 shows the thruster geometry and the computational mesh. The calculated thruster geometry simulates the experimental thruster (flared type)[5,6,16]. The anode is arrayed on the discharge chamber wall and outside wall facing the plume (x = 44 mm and y = 28-40 mm). The cathode is arrayed near the thruster inlet. The calculated region employs the upper half region from the symmetrical plane (y = 0 mm), and consists of the discharge chamber (x = 0 – 44 mm) and the plume region (x > 44 mm). Calculated mesh consists of 50 cells in the x-direction and 30 cells in the y-direction within discharge chamber (x = 0 – 44 mm), and 25 cells in the x-direction and 50 cells in the y-direction within plume region (x > 44 mm). The propellant is injected uniformly from the thruster inlet (x = 0 mm). Six measure points (A-F) of the experiment is referred from Ref. 5.

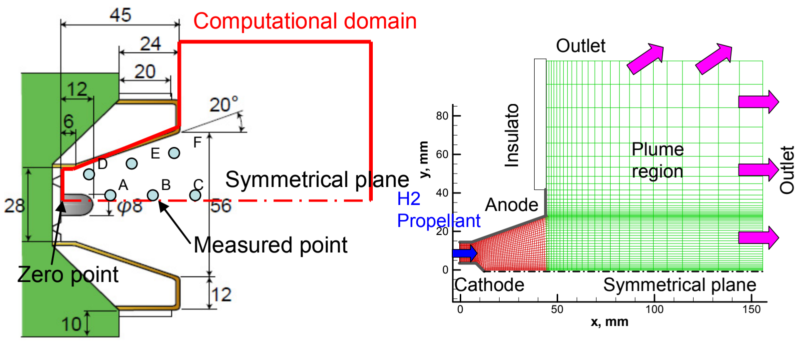

a) Geometry of 2D-MPDT b) Computational mesh

Figure 2 Thruster geometry[5] and computational mesh (thruster width is assumed L_w = 80 mm)

C. Boundary and computational conditions

Table 1 shows the computational and boundary conditions. This computational condition is set same value of the past experimental condition[5,6]. In the inflow condition, the prescribed mass flow rate of hydrogen propellant is 0.65 g/s, and the static pressure is extrapolated from the neighboring cell center. Three temperatures, the dissociation fraction α_{diss}, and ionization fraction α are specified at the inlet. The distribution of the magnetic flux density in y-direction at the inlet is obtained from Ampère's law, that is $B_{z,in} = -\mu_0 J_{dis}/2L_w$. The total discharge current J_{dis} is 13 kA The adiabatic condition is employed on the anode and the cathode. The magnetic flux density on the electrodes is obtained from the following equation (normalized form).

$$\frac{\partial B_z}{\partial \xi}\left[-\beta_{ec}B_z\left(\xi_x^2+\xi_y^2\right)\right]+\frac{\partial B_z}{\partial \eta}\left[\xi_x\eta_y-\xi_y\eta_x-\beta_{ec}B_z\left(\xi_x\eta_x+\xi_y\eta_y\right)+S'B_z^2\left(\xi_x\eta_y-\xi_y\eta_x\right)\right] + R_m B_z\left(\xi_y u_x-\xi_x u_y\right)=0 \tag{18}$$

This equation expresses the condition that the electric field along the wall is zero ($E_\xi = 0$). The discretized Eq. (18) can be written as the cubic formula of B_z which is solved by the Newton-Raphson method in each time step. In this equation, the normalized ion-slip parameter S' is obtained from the following equation.

$$S' = (1-\alpha)^2\beta_{ec}\beta_{ic} = (1-\alpha)^2\frac{\sigma B_{ref}}{e n_e}\frac{e B_{ref}}{m_i \nu_{in}} \tag{19}$$

Table 1 Boundary and computational conditions.

$\dot{m}$, g/s	0.65
J_{dis}, kA	13
T_{tr}, K @ inlet	2,000
T_{vib}, K @ inlet	2,000
T_e, K @ inlet	2,000
α% @ inlet	0.01%
α_{diss}% @ inlet	0.1%
T_{tr}, T_{vib}, T_e @ electrode	Adiabatic

IV. Numerical Results and Discussion

A. Comparison between numerical and experimental results

In this section, we validate the numerical results. Figure 3 shows the discharge current path which the labeled values on the contour lines denote the ratio of the current flowing downstream viewed from the line to the total discharge current. Unlike the measured result (Fig. 3 (a)), in the numerical result without the ion-slip effect (Fig. 3 (b)), the discharge current path of 40 and 60% flows in parallel with the anode near the anode surface (x = 22 - 44 mm) and the discharge current path of 60 and 80% concentrates the anode corner x = 45 mm due to the Hall effect. Hall parameter β_e, which indicates strength of the Hall effect, shows 5.52 – 11 along the anode surface x = 22 – 44 mm. Therefore, in the numerical result without the ion-slip effect, the Hall effect notably appears compared with the measured result. On the other hand, in the numerical result with the ion-slip effect (Fig. 3 (c)), the discharge current path closes in the measured result. In Fig. 3 (c), the concentrate of the discharge current is disappeared, and the entire discharge current path shifts to the downstream, because the discharge current path on the anode surface is raised by the ion-slip effect. The detailed is discussed in the following section.

Figure 4 shows the contour of the electron temperature. In the measured result, the electron temperature is kept approximately constant value at three measured points D-F. In the numerical result without the ion-slip effect, the electron temperature achieves locally high temperature (= 3.2 eV) at the point D. In the numerical result with the ion-slip effect, the electron temperature is decreased to 2.7 eV at the point D, because the part of the electron energy is absorbed by the energy for heavy particle and the discharge current path shifts to the downstream. As a result, the electron temperature is kept approximately constant value at three points D-F in the numerical result with the ion-slip effect.

Figure 5 shows the contour of the translational temperature T_{tr} for heavy particles. At the points B-F, T_{tr} in the numerical result without the ion-slip effect (Fig. 5, (b)) is lower than that in the measured result (Fig. 5, (a)). On the other hand, T_{tr} at the entire points in the numerical result with the ion-slip effect is higher than that in the numerical result without the ion-slip effect, because T_{tr} is heated by the ion-slip effect (the third term of the R.H.S. in Eq. (4)). T_{tr} at the points B-F in the numerical result with the ion-slip effect, however, is lower than that in the measured result, because the anomalous heating model is not considered in this numerical simulation. The other researches[5,18] noted that the anomalous phenomenon (e.g. anomalous heating). Although the anomalous heating model for the hydrogen plasma has been not proposed yet, it is not important for this study because this study focuses the influence of the ion-slip effect on the hydrogen plasma flow field.

Table 2 shows the thruster performance. The numerical thrust F and the input power P_e, respectively, are obtained from the following equations.

$$F = \int_{exit} \left(\rho u^2 + p\right) dS \tag{20}$$

$$P_e = \iint_{vol} \mathbf{j} \cdot \mathbf{E} dV \tag{21}$$

Both the numerical thrust and the input power without the ion-slip effect are lower than measured result. On the other hand, the calculated thrust with the ion-slip effect closes in the measured result, because the input power is increased by the ion-slip effect and then the aerodynamic thrust also increases with the input power. Although the input power with the ion-slip effect closes the measured result, the difference between the calculated with the ion-slip effect and the measured input power is shown because the sheath voltage and the anomalous resistivity are not considered in this numerical simulation. The model of the sheath voltage and the anomalous resistivity should be considered in the future work. In this section, we confirmed that the reproduced precision can be improved by the considering the ion-slip effect.

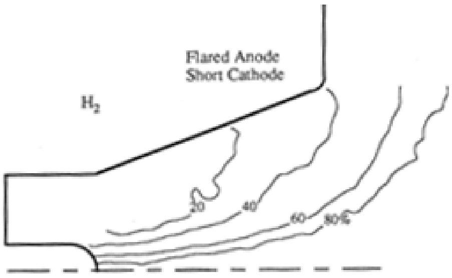

a) Measured result.

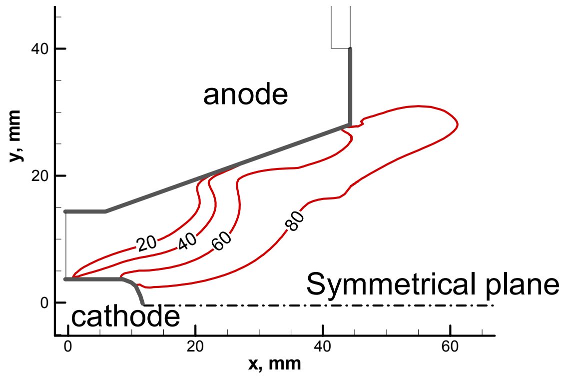

b) Calculated result (w/o ion-slip effect).

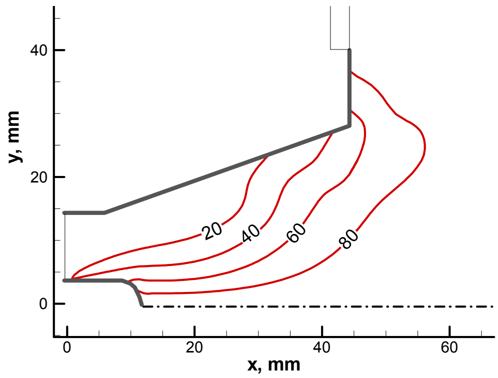

c) Calculated result (with ion-slip effect).

Figure 3 Discharge current path (H_2, J_{dis} = 13 kA, $\dot{m}$ = 0.65 g/s, measured result is referred from Ref. 16, Labeled values are obtained from 100×(1-B_z^*)%, Here B_z^* represent the normalized magnetic density B_z).

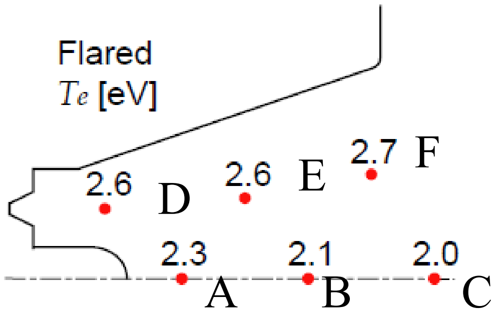

a) Measured result.

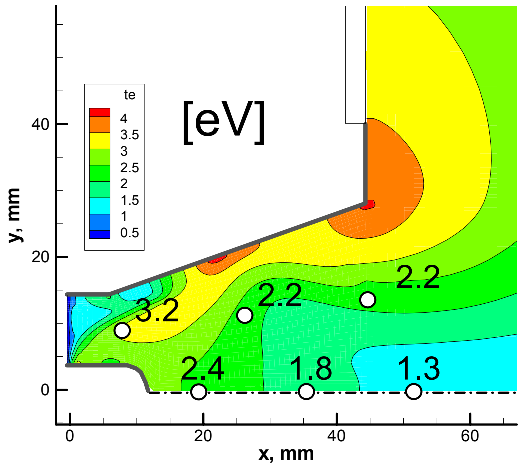

b) Calculated result (w/o ion-slip effect).

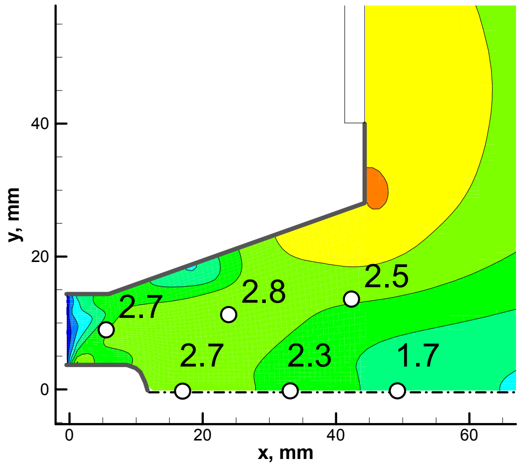

c) Calculated result (with ion-slip effect).

Figure 4 Electron temperature contour (H_2, J_{dis} = 13 kA, $\dot{m}$ = 0.65 g/s, measured result is referred from Ref. 6).

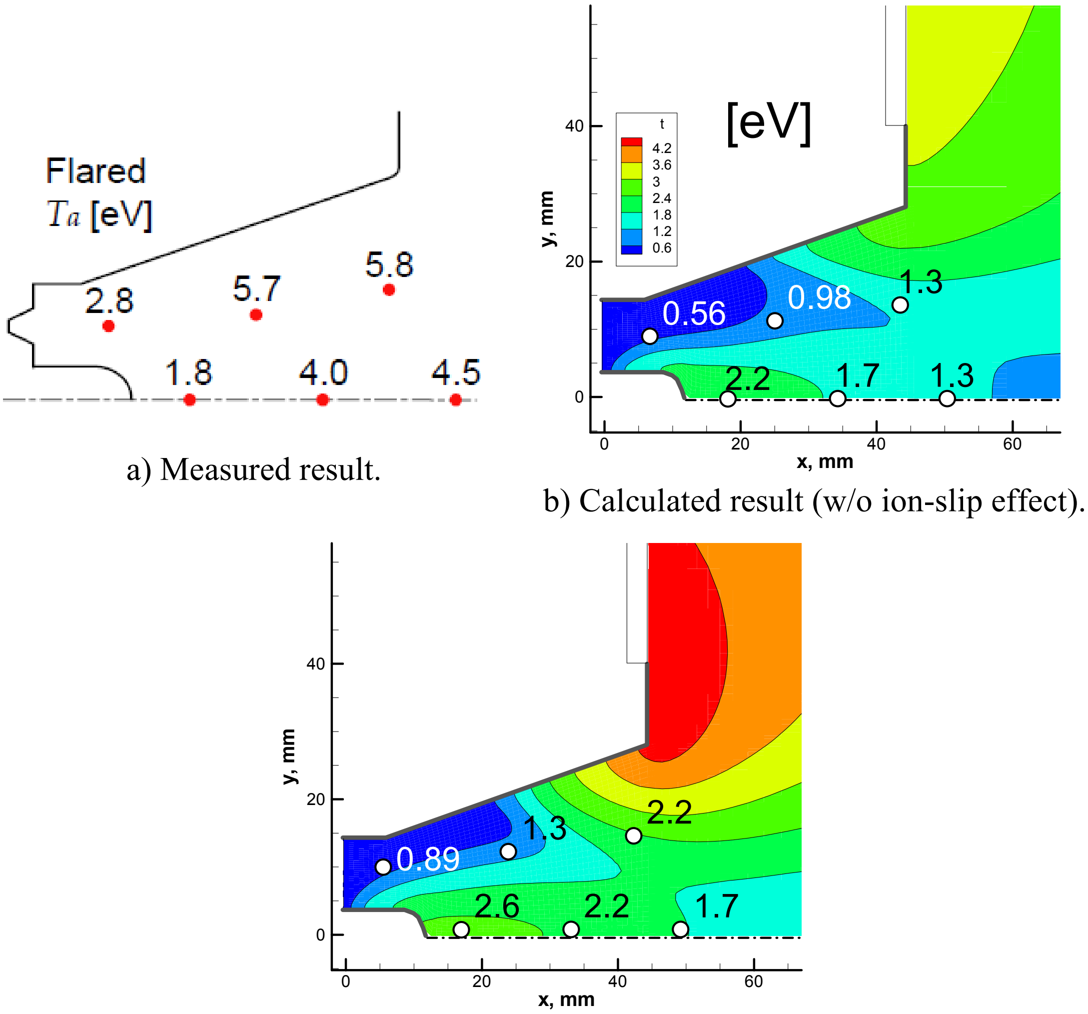

a) Measured result.

b) Calculated result (w/o ion-slip effect).

c) Calculated result (with ion-slip effect).

Figure 5 Translational temperature for heavy particles (H_2, J_{dis} = 13 kA, $\dot{m}$ = 0.65 g/s, measured temperature[6] shows translational temperature for hydrogen atom).

Table 2 Measured[5] and numerical thrust performance(H_2, J_{dis} = 13 kA, $\dot{m}$ = 0.65 g/s)

	F, N	P_e, kW
Measured	27.0	1,521
Calculated (w/o ion-slip effect)	17.4	600 (w/o sheath)
Calculated (with ion-slip effect)	22.1	951 (w/o sheath)

B. Cause of ion-slip effect and influence of ion-slip effect on hydrogen plasma flow field

In this section, the cause of the ion-slip effect and the influence of the ion-slip effect on the hydrogen plasma flow within the MPDT are discussed. Figure 6 shows the contour of the ion-slip parameter S_{ion} which indicates the strength of the ion-slip effect. S_{ion} exceeds unity (strong ion-slip effect) near the anode surface x > 23.1 mm, because its plasma flow is kept low ionization degree (α = 3 - 27%, x = 23.1 - 45 mm, anode surface). It is difficult to be ionized for the hydrogen plasma flow due to its dissociation reaction. In addition, the low collision between ions and neutral particle causes the ion-slip effect, because the plasma pressure near the anode (~ 2,000 Pa) is lower than that near the symmetric plane (~ 5,000 Pa) due to the Lorentz force. Figure 7 shows the relationship between the Lorentz force and the plasma pressure near the anode. As a result of the plasma flow is pinched in radial direction, the plasma pressure near the anode is decreased. The *Knudsen number*, however, is kept ~$O(10^{-2})$.

Figure 8 shows the relationship between the discharge current path and two effects (Hall and ion-slip). In the case with only Hall effect (without ion-slip effect), the discharge current is skewed ($\theta > 0$ deg). On the other hand, the discharge current closes in $\theta = 0$ deg in the case with the Hall and the ion-slip effects. Therefore, the discharge current in the numerical result with the ion-slip effect closes in the measured result in Fig. 3.

Figure 9 shows the contour of the ratio of the translational temperature T_{tr} to the electron temperature T_e. In the calculated result without the ion-slip effect, T_{tr} is lower than T_e within the thruster. On the other hand, T_{tr} exceeds T_e ($T_{tr}/T_e > 1$) around the corner of the anode (x = 45 mm, y = 28 mm) in the calculated result with the ion-slip effect, because the heavy particles are heated by the ion-slip effect (the third term of the right hand side in Eq. (4)). The ion-slip effect heats the heavy particles as the friction heat. As a result of the heavy particles are heated, the plasma pressure for the heavy particle p_h in the calculated result with the ion-slip effect is higher than that in the calculated result without the ion-slip effect in Fig. 10. The high plasma pressure increases the thrust in Table 2.

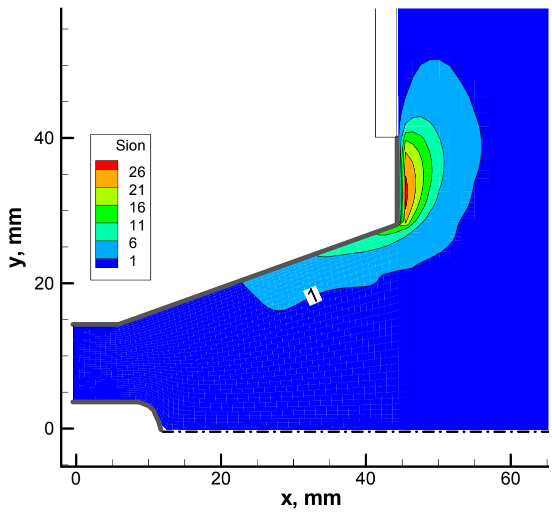

Figure 6 Ion-slip parameter S_{ion} (H_2, J_{dis} = 13 kA, $\dot{m}$ = 0.65 g/s, with ion-slip effect)

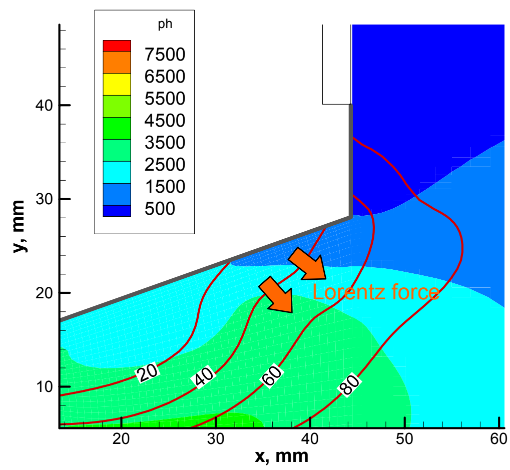

Figure 7 Generating mechanism of ion-slip effect(H_2, J_{dis} = 13 kA, $\dot{m}$ = 0.65 g/s, with ion-slip effect, red line shows the discharge current path)

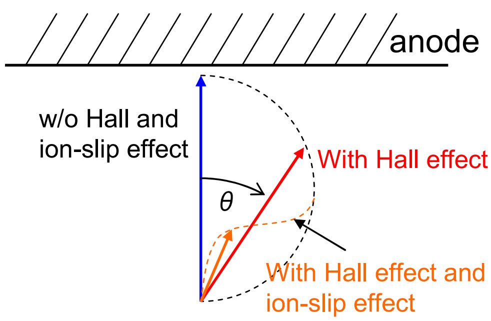

Figure 8 Relation ship between discharge current vector and two effects (Hall effect and ion-slip effect, vector shows the discharge current).

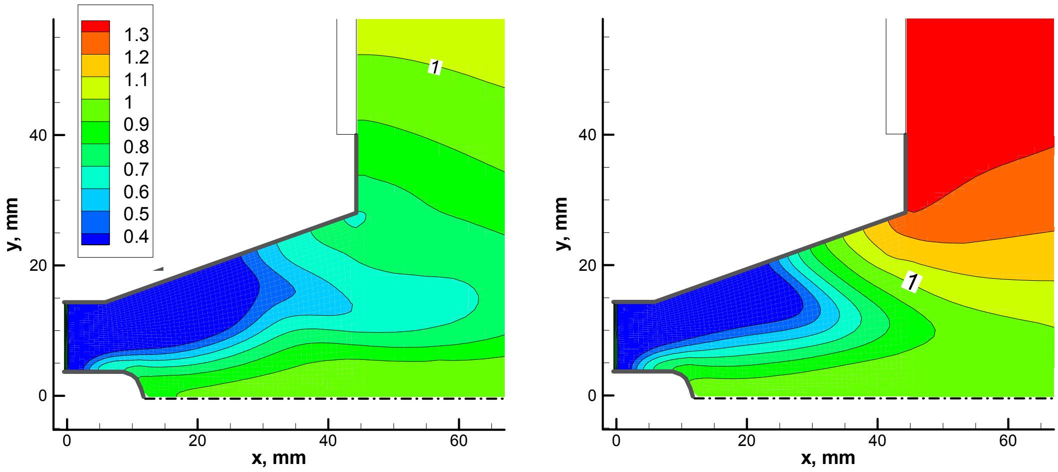

a) Calculated result (w/o ion-slip effect). b) Calculated result (with ion-slip effect).

Figure 9 Ratio of translational temperature for heavy particles to electron temperature T_{tr}/T_e (H_2, J_{dis} = 13 kA, $\dot{m}$ = 0.65 g/s).

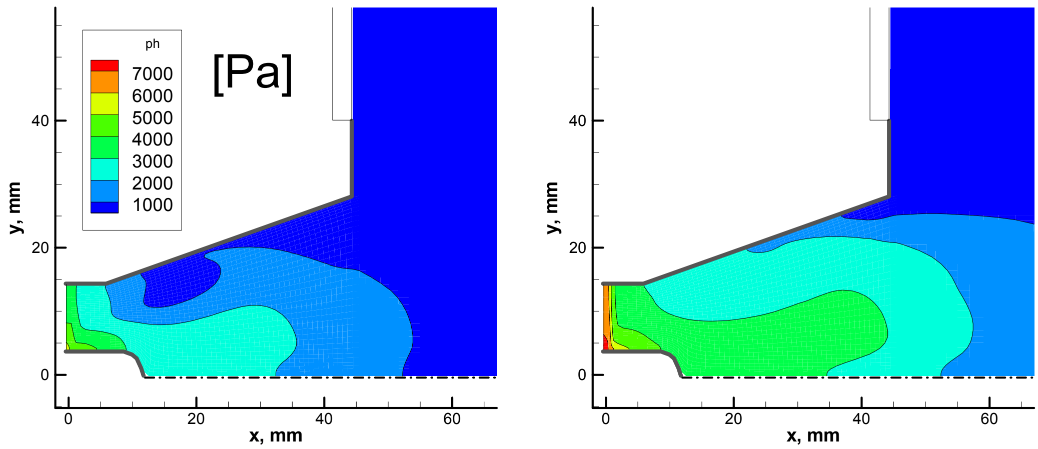

a) Calculated result (w/o ion-slip effect). b) Calculated result (with ion-slip effect).

Figure 10 Pressure for heavy particles (H_2, J_{dis} = 13 kA, $\dot{m}$ = 0.65 g/s)

V. Conclusion

In order to reveal the cause of the ion-slip effect and its influence on the plasma flow within the two-dimensional MPDT using the hydrogen propellant (flared type, $\dot{m}$ = 0.65 g/s, J_{dis} = 13 kA, H_2 propellant), the modeling and the numerical simulation are conducted with the ion-slip effect. Compared to the numerical simulation without the ion-slip effect, the numerical simulation with the ion-slip effect can reproduce the measured result (discharge current path, electron temperature, translational temperature, thrust performance) relatively well. The numerical thrust performance shows F = 22.1 N, P_e = 951 kW (measured F = 27.0 N, P_e = 1,521 kW).

The ion-slip effect causes near the anode (S_{ion} > 1), because the plasma flow is kept low ionization degree and low pressure due to the pinched force. In addition, the translational temperature exceeds the electron temperature around the corner of the anode due to the heating of the ion-slip effect.

Appendix

A. Generalized Ohm's law with ion-slip effect and input power

The generalized Ohm's law with the ion-slip effect is written as the following equation (ignored the gradient of the electron pressure).

$$\mathbf{j}=\sigma(\mathbf{E}+\mathbf{u}\times\mathbf{B})-\frac{\sigma}{en_e}\mathbf{j}\times\mathbf{B}+(1-\alpha)^2\frac{\beta_e\beta_i}{|\mathbf{B}|^2}(\mathbf{j}\times\mathbf{B})\times\mathbf{B} \tag{A.1}$$

The respective third and fourth term expresses the Hall effect and the ion-slip effect. In addition, the electric field is written as the equation.

$$\mathbf{E}=\frac{\mathbf{j}}{\sigma}-\mathbf{u}\times\mathbf{B}+\frac{1}{en_e}\mathbf{j}\times\mathbf{B}-\frac{S_{ion}}{\sigma|\mathbf{B}|^2}(\mathbf{j}\times\mathbf{B})\times\mathbf{B} \tag{A.2}$$

The input power $\mathbf{j}\cdot\mathbf{E}$ is obtained from the following equation.

$$\mathbf{j}\bullet\mathbf{E}=\frac{\mathbf{j}^2}{\sigma}+\mathbf{u}\cdot(\mathbf{j}\times\mathbf{B})+\frac{S_{ion}}{\sigma|\mathbf{B}|^2}(\mathbf{j}\times\mathbf{B})^2 \tag{A.3}$$

The third term expresses the ion-slip effect which is added within the energy conservation for heavy particle. This term heats the heavy particle.

B. Energy conservations with ion-slip effect

The electron energy conservation can be written as the following equation[17].

$$\frac{\partial}{\partial t}\left(\frac{3}{2}p_e\right)+\nabla\cdot\left(\frac{3}{2}p_e\right)\mathbf{u}=-\nabla\cdot\mathbf{q}_e-p_e\nabla\cdot\mathbf{u}-\mathbf{u}\cdot\nabla p_e+\mathbf{j}_e\cdot\mathbf{E}^*+\mathbf{u}\cdot\nabla p_e+Q_{e-s}-Q_e^{ion}-Q_e^{diss} \tag{B.1}$$

The fourth term of right hand side is

$$\begin{aligned}\mathbf{j}_e\cdot\mathbf{E}^*&=(\mathbf{j}-\mathbf{j}_i)\cdot(\mathbf{E}+\mathbf{u}\times\mathbf{B})\\&=(\mathbf{j}-\mathbf{j}_i)\cdot\left(\frac{\mathbf{j}}{\sigma}-\mathbf{u}\times\mathbf{B}+\frac{1}{en_e}\mathbf{j}\times\mathbf{B}-\frac{1}{\sigma|B|^2}(\mathbf{j}\times\mathbf{B})\times\mathbf{B}+\mathbf{u}\times\mathbf{B}\right)\\&=\left(\mathbf{j}-\frac{S}{B^2}\frac{B}{\beta_e}\mathbf{j}\times\mathbf{B}\right)\cdot\left(\frac{\mathbf{j}}{\sigma}+\frac{1}{en_e}\mathbf{j}\times\mathbf{B}-\frac{1}{\sigma|B|^2}(\mathbf{j}\times\mathbf{B})\times\mathbf{B}\right)\\&=\frac{\mathbf{j}^2}{\sigma}\end{aligned} \tag{B.2}$$

Only Joule heating term in the input power of Eq. (A.3) is remained in the energy conservation for electron.

Next, the total energy conservation can be written as the following equation.

$$\begin{aligned}&\frac{\partial}{\partial t}(E_h+E_e)+\nabla\cdot[(E_h+E_e+p)\mathbf{u}]\\&=\mathbf{j}\cdot\mathbf{E}+\nabla\cdot[(\lambda_{tr}+\lambda_{rot})\nabla T_{tr}+\lambda_{vib}\nabla T_{vib}+\lambda_e\nabla T_e]+\nabla\cdot(\bar{\tau}\mathbf{u})-Q_{diss}^h-Q_{diss}^e-Q_{ion}^e\end{aligned} \tag{B.3}$$

Eq. (A.3) is substituted in the first term of the right hand side in Eq.(B.3).

$$\begin{aligned}&\frac{\partial}{\partial t}(E_h+E_e)+\nabla\cdot[(E_h+E_e+p)\mathbf{u}]\\&=\frac{\mathbf{j}^2}{\sigma}+u\cdot(j\times\mathbf{B})-\frac{S_{ion}}{\sigma|\mathbf{B}|^2}(\mathbf{j}\times\mathbf{B})^2+\nabla\cdot[(\lambda_{tr}+\lambda_{rot})\nabla T_{tr}+\lambda_{vib}\nabla T_{vib}+\lambda_e\nabla T_e]+\nabla\cdot(\bar{\tau}\mathbf{u})-Q_{diss}^h-Q_{diss}^e-Q_{ion}^e\end{aligned} \tag{B.4}$$

We subtract the electron energy conservation Eq. (B.1) from Eq.(B.4) to obtain the energy conservation for the heavy particles. The energy conservation of the heavy particles becomes

$$\begin{aligned}&\frac{\partial}{\partial t}(E_h)+\nabla\cdot[(E_h+p)\mathbf{u}]\\&=p_e\nabla\cdot\mathbf{u}+\mathbf{u}\cdot(\mathbf{j}\times\mathbf{B})+\frac{S_{ion}}{\sigma|\mathbf{B}|^2}(\mathbf{j}\times\mathbf{B})^2+\nabla\cdot[(\lambda_{tr}+\lambda_{rot})\nabla T_{tr}+\lambda_{vib}\nabla T_{vib}]+\nabla\cdot(\bar{\tau}\mathbf{u})-Q_{e-s}-Q_{diss}^h\end{aligned} \tag{B.5}$$

In this numerical simulation, the vibrational energy also is considered.

Acknowledgments

This work was supported by the JAXA Super Computer System at the Japan Aerospace Exploration Agency.

References

[1]Sovey, J. S. and Mantenieks, M. A., "Performance and Lifetime Assessment of Magnetoplasmadynamic Arc Thruster Technology," *Journal of Propulsion and Power*, Vol. 7, No.1, 1991, pp.71, 82.

[2]Uematsu, K., Morimoto, S. and Kuriki, K., "MPD Thruster Performance with Various Propellants," *Journal of Spacecraft*, Vol.22, No.4, 1984, pp.412-416.

[3]Tahara, H., Sakakibara, T., Kagaya, Y. and Yoshikawa, T., "Operational Characteristics and Discharge Mechanism of Quasisteady Magnetoplasmadynamic Arcjet for Space Propulsion," *JSPF*, Vol.64, No.2, 1990, pp.195-pp.211. (in Japanese)

[4]Malliaris, A. C., and Libby, D. R., "Spectroscopic Study of Ion-Neutral Coupling in Plasma Acceleration," AIAA Journal, Vol. 9, No.1, 1970, pp. 160, 167.

[5]Kinefuchi, K., Funaki, I., and Toki, K., "Laser Absorption Velocimetry of Plasma Flow in Two-Dimensional Magnetoplasmadynamic Arcjet," Vol. 22, No. 5, 2006, pp.1085, 1090.

[6]Kinefuchi, K., Funaki, I., and Toki, K., "Nozzle Shape Effects On Velocity Distribution in an MPD Arcjet, " *International Electric Propulsion Conference*, IEPC-03-0056, 2003.

[7]Miyasaka, T., Fukuoka, N, and Fujiwara, T, "Numerical Analyses of MHD Flows Based on a Two-Fluid Model in MPD Thrusters," *Journal of the Japan Society for Aeronautical and Space Sciences*, Vol. 48, No. 561, 2000, pp.36 ,42. (in Japanese)

[8]Niewood, E. H., and Martinez-Sanchez, M., "Quasi-One-Dimensional Numerical Simulation of Magnetoplasmadynamic Thrusters," *Journal of Propulsion and Power*, Vol. 8, No. 5, 1992, pp.1031-1039.

[9]Fujita, K. and Arakawa, Y., "Performance Computation of a Low-Power Hydrogen Arcjet," *Journal of Propulsion and Power*, Vol. 15, No.1, 1999, pp.144-150.

[10]Shoji, T. and Kimura, I. "Analytical Study on the Influence of Nonequilibrium Ionization for Current Flow Pattern and Flow Field of MPD Arcjets," AIAA paper 90-2609, 1990.

[11]Mitchner, M., and Kruger, C. H., *Partially Ionized Gas*, John Wiley & Sons, Inc., 1973.

[12]Gnoffo, P. A., Gupta, R. N. and Shinn, J. L. "Conservation Equations and Physical Models for Hypersonic Air Flows in Thermal and Chemical Nonequilibrium," NASA TP-2867, 1989.

[13]Yos, J. M., "Transport properties of nitrogen, hydrogen, oxygen, and air to 30,000°K," , RAD-TM-63-7, 1963.

[14]Stallcop, J. R., Levin, E. and Partridge, H., "Transport Properties of Hydrogen," *Journal of Thermophysics and Heat Transfer*, Vol. 12, No.4, 1998, pp.514-519.

[15]Kubota, K., Doctor thesis, Tokyo Institute of Technology, 2009.

[16]Funaki, I., Doctor thesis, University of Tokyo, 1995.

[17]Sutton, G. W., and Sherman A., *Engineering Magnetohydrodynamics*, Dover Publications, Inc., New York, 2006.

[18]Choueiri, E. Y., and Okuda, H., "Anomalous Ionization in the MPD Thruster," *International Electric Propulsion Conference*, IEPC-93-067, 1993.